

The Herschel/PACS 2560 bolometers imaging camera

Nicolas Billot^a, Patrick Agnèsè^b, Jean-Louis Auguères^a, Alain Béguin^b, André Bouère^a, Olivier Boulade^a, Christophe Cara^a, Christelle Cloué^a, Eric Doumayrou^a, Lionel Duband^c, Benoît Horeau^a, Isabelle Le Mer^a, Jean Le Pennec^a, Jérôme Martignac^a, Koryo Okumura^a, Vincent Revéret^d, Marc Sauvage^a, François Simoens^b and Laurent Vigroux^e

^aService d'Astrophysique, DAPNIA, CEA Saclay, 91191 Gif sur Yvette, FRANCE;

^bLaboratoire Infra-Rouge, LETI, CEA Grenoble, 38054 Grenoble, FRANCE;

^cService des Basses Températures, DRFMC, CEA Grenoble, 38054 Grenoble, FRANCE;

^dEuropean Southern Observatory, Vitacura, Casilla 19001 Santiago 19, CHILE;

^eInstitut d'Astrophysique de Paris, 75014 Paris, FRANCE

ABSTRACT

The development program of the flight model imaging camera for the PACS instrument on-board the Herschel spacecraft is nearing completion. This camera has two channels covering the 60 to 210 microns wavelength range. The focal plane of the short wavelength channel is made of a mosaic of 2x4 3-sides buttable bolometer arrays (16x16 pixels each) for a total of 2048 pixels, while the long wavelength channel has a mosaic of 2 of the same bolometer arrays for a total of 512 pixels. The 10 arrays have been fabricated, individually tested and integrated in the photometer. They represent the first filled arrays of fully collectively built bolometers with a cold multiplexed readout, allowing for a properly sampled coverage of the full instrument field of view. The camera has been fully characterized and the ground calibration campaign will take place after its delivery to the PACS consortium in mid 2006. The bolometers, working at a temperature of 300 mK, have a NEP close to the BLIP limit and an optical bandwidth of 4 to 5 Hz that will permit the mapping of large sky areas. This paper briefly presents the concept and technology of the detectors as well as the cryocooler and the warm electronics. Then we focus on the performances of the integrated focal planes (responsivity, NEP, low frequency noise, bandwidth).

Keywords: bolometers, cryocooler, far infrared, imaging camera, multiplexing, filled bolometer arrays

1. INTRODUCTION

The Herschel Space Observatory is the third “corner stone” mission of the European Space Agency. It will be launched by an Ariane 5 rocket in the course of 2008. Herschel will be equipped with the largest telescope ever sent in space (\varnothing 3.5m) and will carry out spectroscopic and imaging observations in the 60 μ m to 670 μ m wavelength range. Herschel’s payload consists of three instruments. (1) HIFI is a very high resolution heterodyne spectrometer ($R \sim 10^7$), (2) SPIRE is an imager and an imaging spectrometer, operating in the 210-670 μ m band, using spider-web bolometers coupled to Winston cones (see ref. 1 for details), and (3) PACS covers the 60-210 μ m range and is both an imaging spectrometer using photo-conducting detectors, and an imager using novel technology bolometers described in this paper.

The main science objectives of Herschel are twofold. First, Herschel will perform large scale surveys of nearby dark clouds, regions where stars form, in order to identify the mechanisms responsible for the distribution of stellar masses. Indeed we now realize that a star’s mass, when it enters the main sequence, is in fact determined when the gas and dust cloud in which it will later form separates itself from its parent cloud and starts to collapse. At this early stage, it is mostly heated by the contraction and its temperature is such that it radiates most of its energy in the Herschel band. By observing very large numbers of these prestellar cores, we will shed light upon the processes that lead to their formation and to their mass distribution.

Further author information: Nicolas Billot, e-mail: nbillot@cea.fr
PACS Photometer is funded by CNES and CEA.

Herschel will also peer into the distant Universe. Half of the extragalactic background light reaches earth in the infrared, with a peak in Herschel’s bandpass. Herschel will perform deep surveys in dark regions of the sky to identify and locate the galaxies responsible for this background. This will allow the reconstruction of the star formation history of the Universe during the last ~ 10 Gyr. This star formation history is in fact the result of the galaxy formation process, thus Herschel will participate in the construction of a plausible scenario that leads from the very homogeneous Universe of the Big Bang epoch to the highly structured Universe of galaxies that we see now. For more detailed descriptions, see ref. 2 for the Herschel mission, and ref. 3 for the PACS instrument.

2. OVERVIEW OF PHFPU, THE PACS PHOTOMETER

The imaging part of PACS is referred to as the Photometer Focal Plane Unit or PhFPU. It is designed for dual-band imaging in the range 60 to 210 μm . It consists of two channels: the “Blue” one covering the range 60 to 130 μm , and the “Red” one from 130 to 210 μm . The split of wavelength is done with dichroic optics in front of the photometer. The Blue channel is itself split into two sub-ranges, from 60 to 85 μm and 85 to 130 μm by means of a filter wheel. Observations are therefore performed simultaneously in either one of the two blue bands plus the red band (see figure 1 for a picture of the flight model of the photometer).

Each channel has a focal plane based on a mosaic of filled arrays of bolometers (sect. 3): 2048 pixels for the Blue channel (arranged in a mosaic of 4x2 arrays of 16x16 pixels each), and 512 pixels for the Red channel (2 arrays of 16x16 pixels each). The field of view is $3.5' \times 1.75'$ for both channels and is fully sampled by the filled arrays for the central wavelengths. Figure 2 shows the two focal planes of the FM photometer. A cryocooler, based on an ^3He sorption cooler, is used to cool both focal planes to 300 mK (sect. 4).

Each focal plane is mounted inside a structure connected to the 300 mK stage. This structure is itself suspended inside the 2 K structure by means of kevlar wires. A 300 mK filter is mounted on top of each bolometer focal plane. The detectors and their cold readout electronics at 300 mK are electrically connected at the 2 K stage to a second level of electronics. Most of the power is dissipated at this stage since the thermal budget at 300 mK is obviously very tight. Table 1 summarizes the specifications of the photometer.

Spectral range	60 – 210 μm in two channels	
Field of view	$3.5' \times 1.75'$ per channel	
Image quality	Diffraction limited	
Operating temperature	~ 300 mK	
Thermal budget	10 μW at 300 mK	
Autonomy	46 h	
Channels	Blue	Red
Central wavelength	73 or 107 μm	166 μm
Bandwidth $\Delta\lambda$	33 or 43 μm	45 μm
Focal plane	4x2 arrays	2x1 arrays
Number of pixels	2048	512
Pixel field of view	3.2 "	6.5 "

Table 1. Specifications for the PACS photometer.

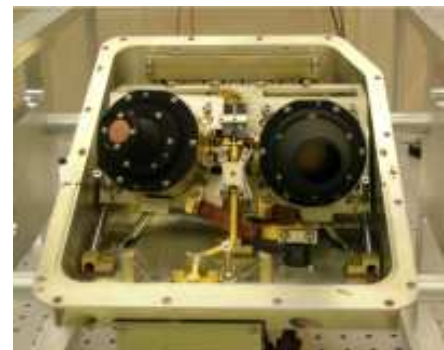


Figure 1. The flight model of the PACS photometer being assembled, Red channel is on the left and Blue on the right. PhFPU dimensions are $260 \times 348.5 \times 216$ mm and its weight is 8.2 kg.

3. THE BOLOMETER ARRAYS

3.1. Detection principle

The PACS bolometer arrays are based on the resonant absorption of the sub-millimeter electromagnetic radiation. In this mode, an absorption layer matched to vacuum impedance ($377 \Omega/\square$) is located above a reflector. In a classical point of view, standing waves generated between incident and reflected radiations allow a theoretical



Figure 2. The Blue (left: 64x32 pixels) and Red (right: 32x16 pixels) FM focal planes.

thermal absorption up to 100% for a wavelength equal to four times the distance between reflector and absorber. This principle introduced by our group in 1996 for detection purposes, is now widely applied in most recent bolometer developments. The metal absorber is deposited on a crystalline silicon mesh insulated from a heat sink by four thin silicon rods ($2\mu\text{m} \times 5\mu\text{m}$ section - $600\mu\text{m}$ long). The time constant of the detector is given by the heat capacity of the insulated structure and the thermal conductance of the rods. To lower as much as possible the heat capacity of the sensitive part of the bolometer (the insulated structure), we act on both components of the heat capacity: mass and specific heat. Reduction of the mass is obtained by thinning the silicon support to a limit compatible with the process technology ($5\mu\text{m}$). Subsequent etching of the silicon layer, to produce a mesh, achieves the mass reduction process. Specific heat of crystalline materials drops rapidly when lowering temperature below 1 K. We take advantage of this physical property by running detectors below 300 mK. The specific heat of metals and amorphous materials decreases less rapidly. A metal alloy in the superconductor state (titanium nitride), far from the transition, is chosen as absorber to bypass this drawback. The temperature elevation of the sensitive part must be measured. A semiconductor thermometric structure is fitted out on the mesh. This structure is a thin ($<1\mu\text{m}$) and elongated silicon layer heavily doped with phosphorus and 50% compensated by boron ions, electrically insulated from the mesh. This thermometer structure was measured to be the most significant part of the heat capacity of the sensitive part of the detector.

3.2. Description of the bolometer arrays

The way to collectively build large filled arrays while satisfying all the prescriptions outlined above is to use two silicon chips: one containing the absorbing insulated meshes with thermometers (the pixels) and the other containing the reflectors and the cold readout electronics. We then hybridize both with well defined indium bumps to achieve the resonant cavity. Double Silicon On Insulators (SOI) wafers are used for detectors layers. Deep etching ($400\mu\text{m}$) in one direction, and surface etching ($6\mu\text{m}$) in the other produce meshes and rods on the metallized silicon surface. Before that, surface etching of the heavily doped silicon layer produces the mesa structure of the thermometer. This structure is electrically insulated from the mesh by the wafer SiO_2 upper insulation level. Detectors of large sensitive surfaces are thus produced with sufficiently low heat capacity to avoid any light concentrator as needed in classical bolometric cameras. This solution opens the way for filled arrays collective production.

The second chip to be hybridized is also a silicon integrated circuit. It carries on its surface the gold reflectors covering C-MOS readouts and multiplexing circuits. C-MOS (N&P) transistors circuits were adopted there to ensure electric functions at the detectors operating temperature of 300 mK. As the noise density for these circuits is large, with respect to FET transistors, we decided to run thermometers at very high resistance (in the $\text{T}\Omega$ range) to ensure large signals. FET transistors, inefficient below 100 K, cannot be used in our case. The disadvantage of $\text{T}\Omega$ circuits is the difficulty to propagate signals on significant distances. The proximity of the hybridized stages (a few millimeters) relaxes the problem.

Chips including 16 x16 pixels and chips including 16 x16 MOS readout circuits are manufactured for proper combination leading to sub-units of 256 detectors. These sub-units are designed to be butttable on three sides

for large focal planes assembly.

The wavelength absorption requirement was initially ensured by two sizes of indium bumps (20 and 25 μm), according to calculations. Spectral reflection measurements with a Fourier Transform Spectrometer showed that the shorter bump size is sufficient to cope with both wavelength range requirements. Only the “20 μm ” type associated to the Blue channel was then manufactured.

A large focal plane containing 2560 bolometers is not really compatible, in a space project, with a “one readout channel per detector” policy and multiplexing is therefore mandatory. This function is ensured by MOS transistors used here as gates at the readout chip level. A 16 to 1 multiplexing is now currently achieved reducing the total output channels to 160. Frames are then produced at 40 Hz.

The power dissipation available at the 300 mK level is very low ($10\mu\text{W}$). The only way to meet this requirement is to output the bolometer signals from the 300 mK readout stage into the $\text{M}\Omega$ range. When including the multiplexing to the frame frequency, the available length range is of the order of ten centimeters. A second readout stage (impedance adaptation) is then provided a few centimeters away on a part of the focal plane linked to the satellite 2 K level. There, 3.5 mW of power is available and sufficient to transfer signals to the warm electronics.

Figure 3 shows the structure of the bolometer pixel, while figure 4 shows a close-up view of a bolometer array. More details on the technology of these bolometer arrays can be found in reference 4.

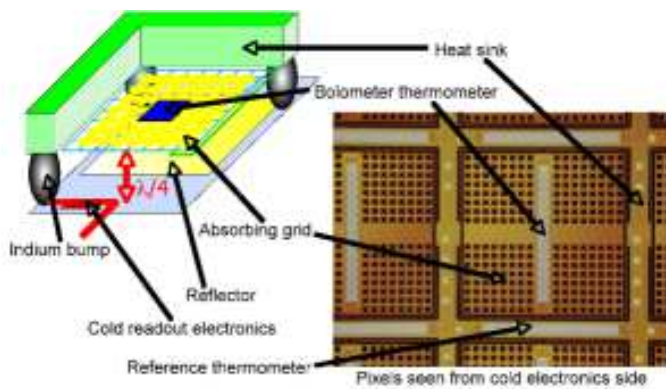


Figure 3. Structure of a bolometer pixel. Pixel step is 750 μm .

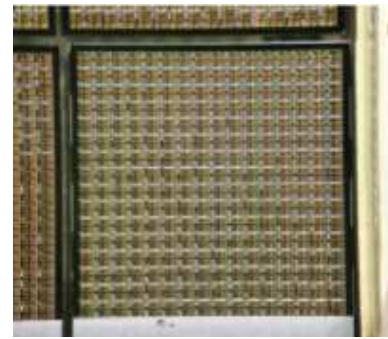


Figure 4. View of an array integrated in the Blue focal plane showing 256 multiplexed bolometers. Array dimensions are 12.63×15.78 mm.

3.3. Irradiations

A “total ionizing dose” measurement was performed using a ^{60}Co gamma ray source. The purpose was to observe any damage due to protons and electrons after an irradiation level equivalent to the expected cumulated ionizing dose at the end of the mission (11 krad). No significant degradation, either in thresholds or gains of the bolometer arrays, has been observed, and the detectors can withstand the spatial environment without degradation of their performances.

Another irradiation run was performed to look for single event effects: proton and alpha irradiations were performed at the Institut de Physique Nucléaire (IPN, Orsay, France), respectively at 20 MeV and 30 MeV with fluences of ~ 3 particle/sec/pixel and ~ 0.2 particle/sec/pixel on a dedicated bolometer array representative of the flight model. We observed no significant variation of the gain of the detector. The main effects were threshold shifts and glitches (see figure 5). Threshold shifts can be explained by the passage of particles through the CMOS cold readout electronics located just below the detection layer. However most of the perturbations were glitches due to the passage of ions through the absorbing mesh resulting in a temperature increase of the pixel. These caused a rapid signal variation, with an average duration of about 4 frames (at a frame rate of 40 Hz) and an amplitude ranging from 1 mV to 60 mV with a mean value of about 10 mV. A preliminary analysis shows a spatial distribution of the incident particle signatures (number of frames affected, or relaxation time) correlated with the responsivity map of the pixels (or the bolometer impedances at first order).

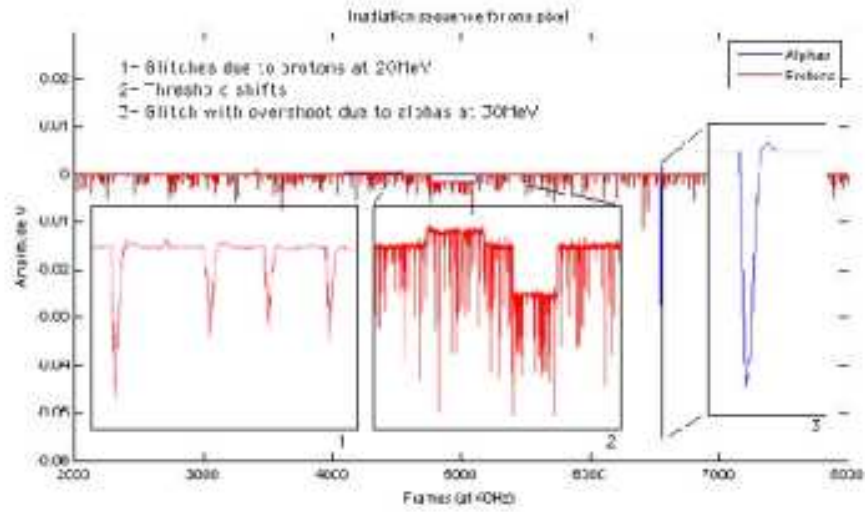


Figure 5. Different effects of alpha and proton impacts on the bolometers.

4. THE CRYOCOOLER

The SPIRE and PACS instruments on-board the Herschel spacecraft have the same sorption coolers, which are based on an ^3He evaporative cooling cycle. The units have been designed following the same overall specifications (see table 2). They feature the same mechanical interface and if necessary can be swapped with a few minor adjustments.

Table 2. Herschel cooler specifications.

Safety	Structural failure mode shall be leak before burst
Mechanical (worst case axis)	Sine sweep vibration: 22.5 G peak up to 100 Hz Random 20 – 150 Hz: 11.5 G rms First eigenfrequency above 120 Hz Proof pressure: 2 x maximum operating pressure
Thermal	Heat lift capability: 10 μW minimum at 290 mK 5 Joules of gross cooling energy at 300 mK Recycling time: no more than 2 hours Total energy dissipated per cycle: no more than 860 J
Electrical	Cold interface (cooler heart) electrically insulated from mechanical interfaces
Geometry and Interface	Volume and Mass: 100x100x230 mm maximum – < 1.8 Kg Mechanical interface: with a 4 K structure Thermal interface: with a 1.7 K ^2He bath

The thermal architecture in the satellite is such that the coolers are mechanically mounted off a structure at 4 K or above (“level 1”) and thermal paths are then provided to the superfluid tank (“level 0”) for the cooler operation. This constraint calls for a specific thermal architecture and design. In addition during cooler operation, in particular during the recycling phase, the heat flows to the tank from the sorption pump and from the evaporator are significantly different. During this phase it is crucial to keep the evaporator temperature as cold as possible to increase the condensation efficiency and reduce the fraction of liquid lost during cooldown. Consequently two thermal interfaces and thus two thermal buses to the superfluid tank are required. Finally to fulfil the electrical insulation requirement, two gas gap heat switches are mounted on the mechanical frame

/ thermal heat sink. Additionally a separate specific enclosure contains the power related function (Power Supply Unit).

BOLC dimensions are $382.5 \times 289 \times 333.5$ mm and its weight is 18.25 kg. The power budget of the warm electronics is 44.2 W in nominal operation mode (i.e. observing), 6.9 W during recycling and 6.0 W in stand-by.

5.1.1. Analog Signal Processing

The analog signal processing chain is divided into several stages: two are part of the detector assembly: the cold readout electronics (at 300 mK) and the cold buffer (at 2 K), as shown in figure 8.

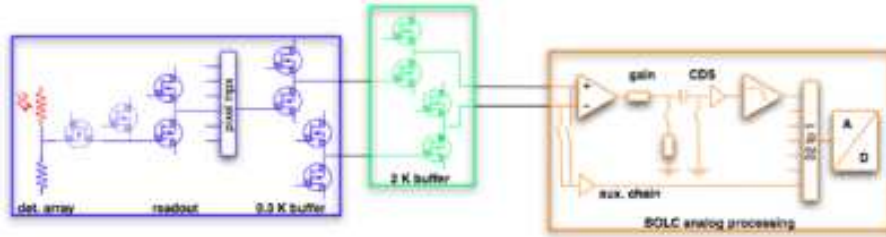


Figure 8. The PhFPU analog electronics.

The last stage (at warm temperature) is within the BOLC unit. The instantaneous dynamic range is determined by the analog to digital converter limited by cold electronics transfer function mismatches: a value of 65000 can be considered. The full dynamic range takes advantage of the gain switching and of the detector noise over-sampling and reaches a value of 330000 (corresponding to the range from 3 mJy to 1000 Jy for incident optical flux). A total number of 5 modules is required to process the 160 bolometer signal outputs: 4 dedicated to the Blue focal plane and 1 to the Red focal plane. Limited power budget for the whole unit implies the design of very low power analog channel while keeping low noise performance: measurement on the flight model gives a value of 9.4 mW per readout channel.

5.1.2. Detector clock sequencer and bias generator

BOLC contains adjustable voltage generators and clock translators required to bias and address a bolometer array. All the parameters are controlled by means of low level commands via digital module allowing for optimization of the bolometer performance, according to initial cold electronics parameter dispersion, detector illumination and parameter drift during instrument life.

A total of 3 modules is required to handle independently 4 groups of 2 arrays for the Blue focal plane and 2 groups of 1 array for the Red focal plane respectively, corresponding to the setting of more than 100 parameters, no less than 19 biases and clocks being required for each detector. The module implementation includes 12-bit digital to analog converters for adjustable settings, analog switches for on/off functions while the digital functions are embedded into a single radiation tolerant FPGA (RT1425 from ACTEL).

Clock translators are driven by a programmable sequencer: timing can be trimmed by means of telecommands to optimize detector performance. An additional signal is provided to the rest of the instrument to achieve the synchronization of the PACS chopper with the bolometer frame readout. The sequencer is implemented in the FPGA along with other functions of the digital module. To perform quick interface checking, the sequencer also features an internal pseudo random data generation allowing data generation even if unplugged from the PhFPU cold electronics.

5.1.3. Ultra low temperature measurement

BOLC also controls the cryocooler and the acquisition of the housekeeping parameters, including measurements of the photometer temperature. Detector and cryocooler operations require various PhFPU temperatures to be monitored and the measurements cover a range from 0.2 K to 50K. Lower temperature measurements (0.2 K to 1 K) require a very high resolution (0.0001 K). For such measurements the probe bias must be chosen to

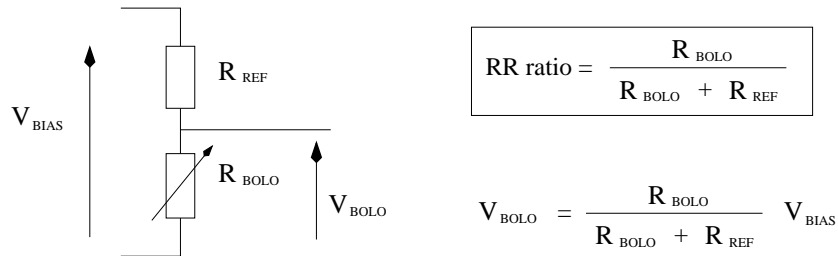


Figure 9. Electrical setup of the bolometric bridge for a single pixel (left). Definition of the RR ratio and the corresponding expression for V_{BOLO} (right).

maximize sensitivity and to limit self heating ($P_{probe} < 1\text{ nW}$). Even higher resolutions ($10\ \mu\text{K}$) can be achieved by accumulating samples over one second.

5.1.4. SpaceWire digital interface

The digital module handles analog module communications as well as external communication with the PACS warm electronics based on a single Command and Data interface running over the SpaceWire standard. The SpaceWire core has been developed in order to optimize design integration. Thus all the digital functions of the BOLC unit have been embedded into a single radiation tolerant RT54SX32S FPGA from ACTEL .

5.1.5. Redundancy

Standard safety considerations have been taken into account in order to deal with electronics failures: single point failures are avoided and failure propagations are minimized. Unit internal redundancy relies on both cold and warm redundancies: analog functions are shared into 6 independent modules each being devoted to a bolometer sub-assembly (warm redundancy) while digital functions (clock sequencer, interfaces to PACS instrument, internal interfaces to analog functions) are doubled (cold redundancy). Therefore a failure at analog electronics level is limited to a portion of the field of view and recovery from a failure in digital electronics is simply achieved by switching from main to redundant module.

6. PERFORMANCES OF THE PHOTOMETER FOCAL PLANE UNIT

Delivery of the Photometer to the PACS consortium at the Max Planck Institute for Extraterrestrial Physics (Germany) is scheduled for June 2006. The results presented in this section were obtained in CEA Saclay during the first quarter of 2006 while preparing for the calibration campaign and deal mainly with performance optimizations.

6.1. Measuring RR ratios

The bolometric signal, V_{BOLO} , is set at the middle point of a voltage divider, also called bolometric bridge. It consists of a bolometer resistor R_{BOLO} and a reference resistor R_{REF} . Figure 9 shows the electrical setup of the bolometric bridge and the definition of the *RR ratio*. Both resistors are strictly identical*, however the bolometer's temperature, hence its impedance, is allowed to fluctuate with the pixel temperature whereas the reference resistor is in thermal contact with the inter pixel wall which acts as the 300 mK heat sink (figure 3). In this configuration the reference resistor is used as a current source for the bolometer and prevents any burnout phenomenon. Note that typical voltages applied across the resistors are of the order of a few Volts which induces electric field effects in the conduction process (impedance decreases with applied voltage).

While most bolometers can be fully characterized by measuring their load curves, we rather use *RR ratios* to determine the state of the bolometric bridge. Indeed the bolometers are multiplexed and each array contains 256 bolometers mounted in parallel so we cannot measure the current flowing through each bolometer individually.

*Same doping, same size ($40 \times 600\ \mu\text{m}$) and impedance of about $0.7\ \text{T}\Omega$ at 300 mK

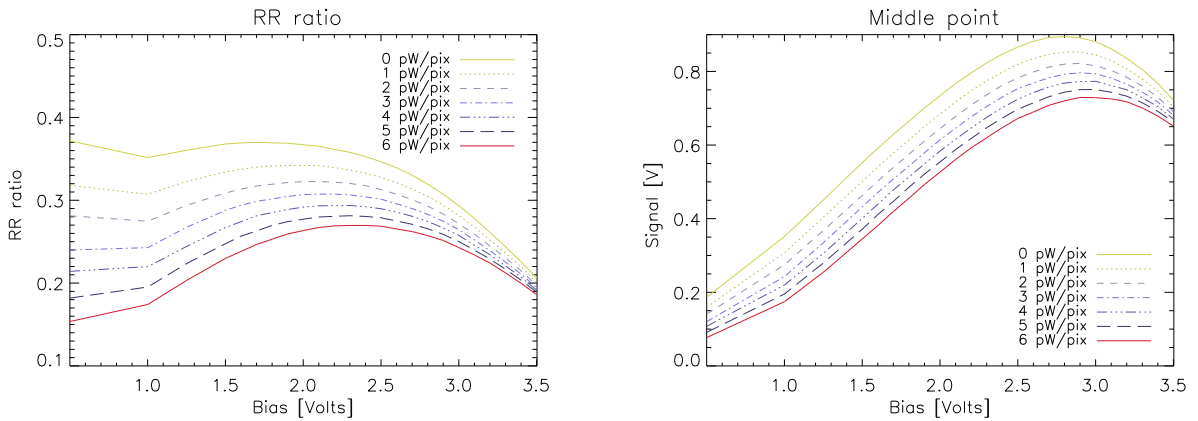


Figure 10. Median RR ratios of a single array plotted versus voltage bias for different background fluxes (left) and the corresponding V_{BOLo} values (right). Top curves corresponds to 0 pW background and bottom curves to 6 pW.

Moreover the 300 mK reference resistor impedance varies with the applied bias due to electric field effects and it cannot be considered as an actual load resistor.

RR ratios are obtained from static measurements with a stable and thermalized black body illuminating the whole focal plane. We record the 40 Hz-sampled signal of each of the 2560 bolometers for 3 minutes in different bias/background flux configurations. In fact each of these configurations requires a different tuning of the detectors to avoid saturation of the signal. Reconstructing RR ratios by taking into account the different offsets and gains of the electronics chain provides us with absolute measurements of the bolometric bridge and makes data obtained in very different conditions comparable. The computation of RR ratios played an important role in understanding the functioning of the bolometer arrays. RR ratios and their corresponding V_{BOLo} values are plotted in figure 10. RR ratios can be interpreted as a competition between the reference and the bolometric resistors and reflect the balance or rather the unbalance of the bolometric bridge.

RR ratio measurements provide us with a large and valuable amount of information. For instance detector responsivity can be derived from the data presented here as described in section 6.2. Moreover we made an extensive use of these ratios to predict the different voltages necessary to power up the detectors[†]. Indeed the middle points being quite dispersed, it is crucial to fine-tune the detectors to ensure all pixels fit in the dynamics of the ADC.

6.2. Responsivity measurements and non-linearity

The responsivity is usually measured by modulating the incident flux with a chopper, the responsivity is then the ratio of the signal amplitude to the flux modulation amplitude. It is expressed in V/W. In our case since RR ratios are reconstructed for different biases and background fluxes we compute $\partial Signal / \partial Flux$ for each pixel and for each flux and bias. Figure 11 shows a responsivity map of the Blue focal plane for a bias of 2.2 V with a background flux of 2 pW/pixel. The responsivity is about 4×10^{10} V/W and is quite homogeneous over the whole focal plane.

Table 4 presents the average responsivity of the Blue focal plane for fluxes in the range 0 to 7 pW/pixel[‡] along with its associated deviation. It shows only a slight non-linearity over this background flux range.

6.3. Spectral noise density and bandpass cutoff frequency

PACS bolometers exhibit noise levels two orders of magnitude higher than “usual” bolometers. This is mainly due to the MOS cold readout electronics located at 300 mK but also to their impedance close to 1 T Ω . We

[†]There is a set of 19 inter-dependant voltages necessary to tune the bolometers of a single array

[‡]We expect a background flux from the telescope between 1 and 6 pW/pixel.

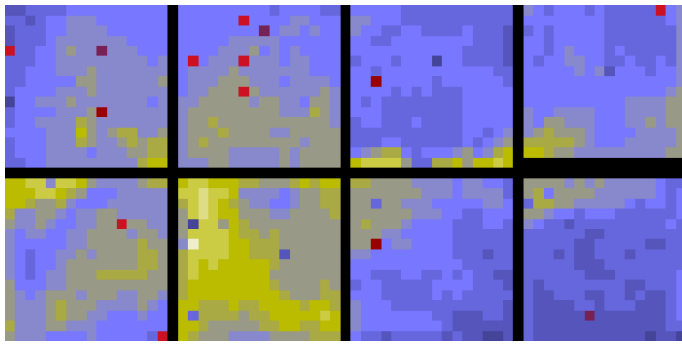


Figure 11. Responsivity map of the Blue focal plane for a background flux of 2 pW/pixel and a bias of 2.2 V.

Background Flux (pW/pix)	Mean Resp. ($\times 10^{10}$ V/W)	σ (%)
0	4.20	20.54
1	4.18	20.49
2	4.15	20.44
3	4.13	20.39
4	4.11	20.34
5	4.08	20.29
6	4.06	20.24
7	4.03	20.18

Table 4. Mean responsivities of the Blue focal plane measured in static mode for different fluxes and its associated relative dispersions.

actually measure noise levels at 3 Hz of about $7 \mu\text{V}\cdot\text{Hz}^{-1/2}$ on the Blue focal plane and $18 \mu\text{V}\cdot\text{Hz}^{-1/2}$ on the Red one. Figure 12 shows the spectral noise density extracted from a 3 hours measurement as well as a histogram of noise levels measured at 3 Hz. The spectrum was obtained by coadding spectra of 4-minutes sub-samples to decrease the statistical fluctuations. Moreover 256 spectra from pixels of the same array have been averaged to obtain the final spectrum representative of the whole array.

We distinguish 3 domains in this spectrum: (1) the low frequency region ($f_{knee} < 0.5$ Hz) concentrates most of the energy and is responsible for signal drifts, (2) the operational regime between 0.5 and 5 Hz which is dominated by photon noise and (3) the white noise filtered by the bolometers electrical time constant ($\tau \sim 60$ ms). Additional bandpass tests confirmed the 5 Hz value for the electrical bandpass cutoff frequency[§] and revealed a thermometric time constant of 20 ms. These time constants can possibly be lowered by increasing the bias.

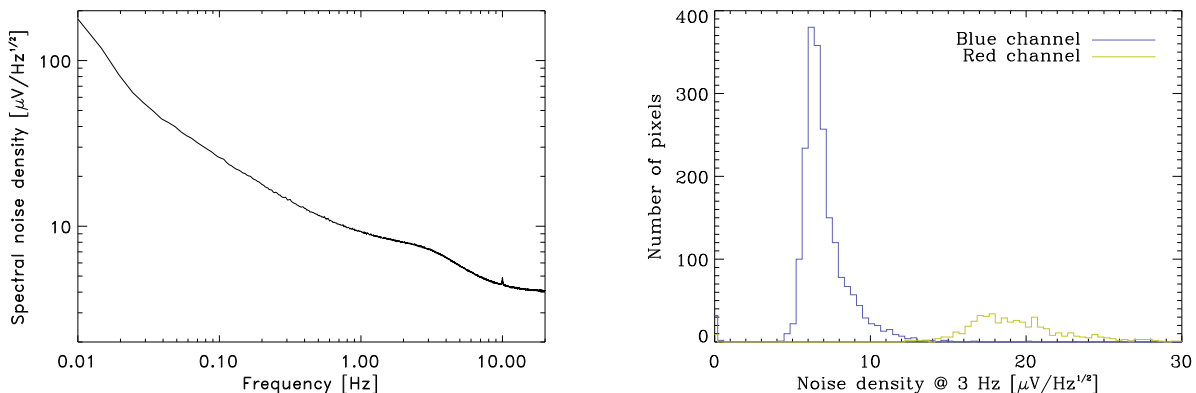


Figure 12. Average noise spectrum of 256 pixels from the same array (right). The histogram showing the noise dispersion on the Blue and Red focal planes.

6.4. Sensitivity measurements

In the sub-millimeter regime, the sensitivity is usually expressed as a NEP (Noise Equivalent Power) and is defined as the ratio of the noise level by the responsivity. We adopt this definition and we find an optimal NEP of $2 \times 10^{-16} \text{ W}/\sqrt{\text{Hz}}$ at $90 \mu\text{m}$ and $3.5 \times 10^{-16} \text{ W}/\sqrt{\text{Hz}}$ at $160 \mu\text{m}$ for a bias of 2 Volts at a background flux of 2 pW/pixel.

[§]The bandpass cutoff frequency is defined as the modulation frequency at which the signal is attenuated by 3 dB.

Again, these results were derived from the data presented in section 6.1. The 3 minutes samples recorded in each configuration were used to compute noise levels at 3 Hz and responsivities were derived from $\partial Signal/\partial Flux$. Figure 13 presents NEP values for fluxes between 1 and 5 pW/pixel as a function of the applied bias. The optimum NEP is reached for a bias around 2 V independently of the background flux. At low biases the Joule dissipation is small and the bolometers are too cold, resulting in a very high impedance and thus high noise levels. At higher biases, bolometers are heated up by Joule dissipation which decreases significantly the impedance and thus the responsivity.

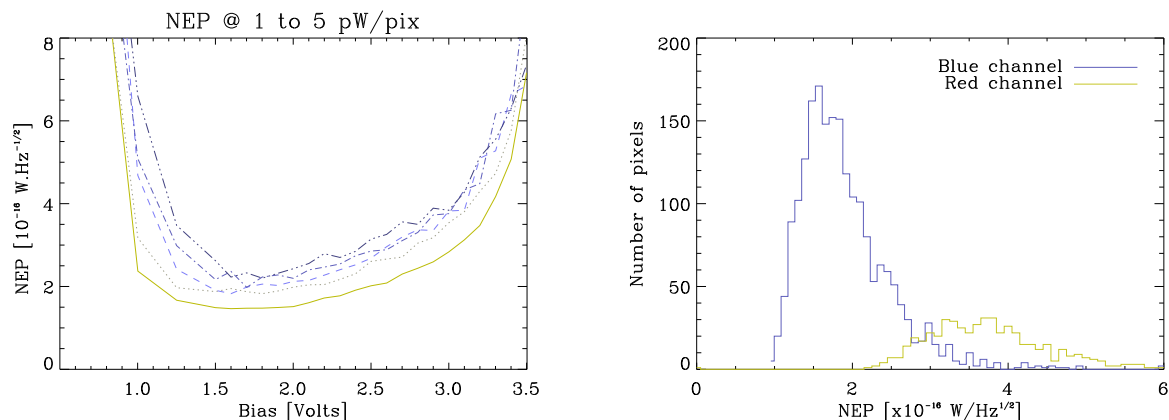


Figure 13. Measured median NEP obtained in static setup (without chopping) for background fluxes of 1 to 5 pW/pixel from bottom to top (left); the corresponding histogram showing the dispersion of NEP on the whole PhFPU for a background of 2 pW/pixel and a bias of 2 V (right).

7. CONCLUSION AND FUTURE DEVELOPMENTS

The development of the bolometers for the Herschel/PACS instrument demonstrates that it is now possible to build fairly large (> 1000 pixels) focal planes based on filled arrays. The grid + resonant cavity concept works, the science requirements on the Blue focal plane have been reached and we will improve the performances of the Red focal plane before delivery to the PACS consortium.

The future of this type of bolometers looks very bright. We have already started a number of developments that will make use of these detectors in the sub-mm and millimeter wavelength ranges, opening the possibility of wide field imaging in these spectral domains. The two main axes of development are (1) to redesign the packaging of the arrays to make them 4-side buttable, opening the way for very large focal planes of bolometers, and (2) to adapt the grid + cavity concept for absorption at longer wavelength.

Table 5 lists the different projects in terms of spectral range, size of focal planes, and telescopes.

Table 5. On-going developments of filled arrays of bolometers.

Name	Spectral range	Focal plane	Telescope	Operational in
P-ARTEMIS	2 channels 200 + 450 μm	1 array per channel	KOSMA + Chile	2006
PILOT	2 channels 240 + 550 μm	2x2 arrays per channel	balloon	2009
ARTEMIS-1	3 bands 200 – 350 – 450 μm	4x4 arrays	APEX	2009
ARTEMIS-2	3 bands 0.85 – 1.2 – 2 mm	4x4 arrays	open (IRAM...)	2010

The adaptation of the bolometers to longer wavelengths is simply a tuning of the depth of the resonant cavity, in order to keep it at a quarter of the wavelength of interest. This tuning can be done in several ways: keeping

the same cavity and putting a dielectric layer with the proper thickness on top of the pixel, inserting a spacer in between the absorbing grid and the reflector to adjust the depth of the cavity, or a mix of these two methods. This adaptation to longer wavelengths is presented in ref. 6, and the ARTEMIS project is presented in greater details in ref. 7.

A first observing run of the P-ARTEMIS camera on the KOSMA telescope occurred in March 2006, which demonstrated that these detectors actually work at longer wavelengths. Figure 14 shows a scanned map of Jupiter taken at $450\ \mu\text{m}$.

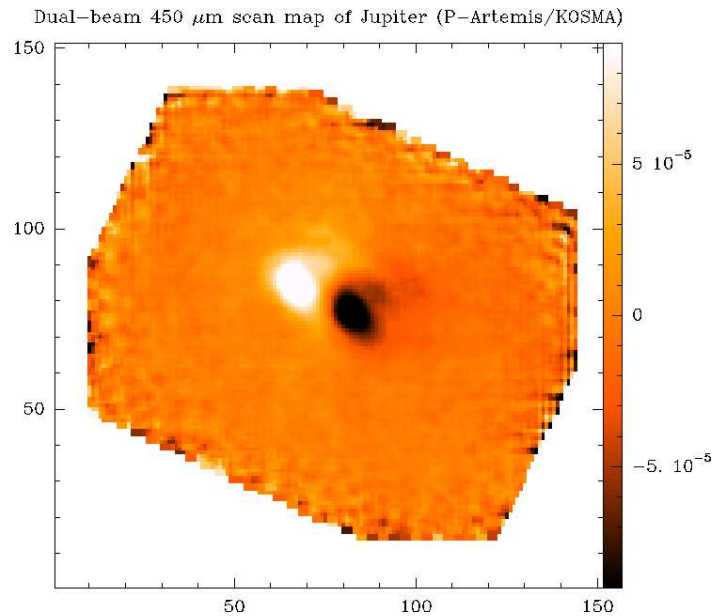


Figure 14. Scanned map of Jupiter at $450\ \mu\text{m}$.

REFERENCES

1. A. D. Turner *et al.*, “Silicon nitride Micromesh Bolometer Array for Submillimeter Astrophysics,” *Applied Optics* **40**, pp. 4921–4932, Oct. 2001.
2. G. L. Pilbratt, “Herschel mission: status and observing opportunities,” in *Optical, Infrared, and Millimeter Space Telescopes. Proceedings of the SPIE, Volume 5487*, pp. 401–412, J. C. Mather, ed., Oct. 2004.
3. A. Poglitsch *et al.*, “The photodetector array camera and spectrometer (PACS) for the Herschel Space Observatory,” in *Optical, Infrared, and Millimeter Space Telescopes. Proceedings of the SPIE, Volume 5487*, pp. 425–436, J. C. Mather, ed., Oct. 2004.
4. F. Simoens *et al.*, “Submillimeter bolometers arrays for the PACS/Herschel spectro-photometer,” in *Millimeter and Submillimeter Detectors for Astronomy II. Proceedings of the SPIE, Volume 5498*, pp. 177–186, J. Zmuidzinas, W. S. Holland, and S. Withington, eds., Oct. 2004.
5. P. Hargrave *et al.*, “The 300mK system for Herschel-SPIRE,” in *Millimeter and Submillimeter Detectors and Instrumentation for Astronomy III. Proceedings of the SPIE, Volume 6275*, J. Zmuidzinas, W. S. Holland, S. Withington, and W. D. Duncan, eds., 2006.
6. V. Revéret *et al.*, “A study on the use of the PACS bolometer arrays on submillimeter ground-based telescopes,” in *Millimeter and Submillimeter Detectors and Instrumentation for Astronomy III. Proceedings of the SPIE, Volume 6275*, J. Zmuidzinas, W. S. Holland, S. Withington, and W. D. Duncan, eds., 2006.
7. M. Talvard *et al.*, “ARTEMIS: filled bolometer arrays for sub-millimeter instrumentation of the next-generation telescopes,” in *Millimeter and Submillimeter Detectors and Instrumentation for Astronomy III. Proceedings of the SPIE, Volume 6275*, J. Zmuidzinas, W. S. Holland, S. Withington, and W. D. Duncan, eds., 2006.